Supporting Information

Resilient Biomass-Derived Hydrogel with Tailored Topography for Highly Efficient and Long-Term Solar Evaporation of High-Salinity Brine

Xiaoxiao Chen [a, c], Zhiying Wu [a, b], Dengguo Lai [a *], Min Zheng [a, b], Lei Xu [a, b], Jiangbo Huo [a], Zhangxu Chen [c], Baoling Yuan [d], Ming-Lai Fu [a, d *]

[a] CAS Key Laboratory of Urban Pollutant Conversion, Institute of Urban Environment, Chinese Academy of Sciences, Xiamen, 361021, China

[b] University of Chinese Academy of Sciences, Beijing, 100039, China

[c] Fujian Provincial Key Laboratory of Ecology-Toxicological Effects & Control for Emerging Contaminants, Putian, 351100, China

[d] College of Civil Engineering, Huaqiao University, Xiamen, 361020, China

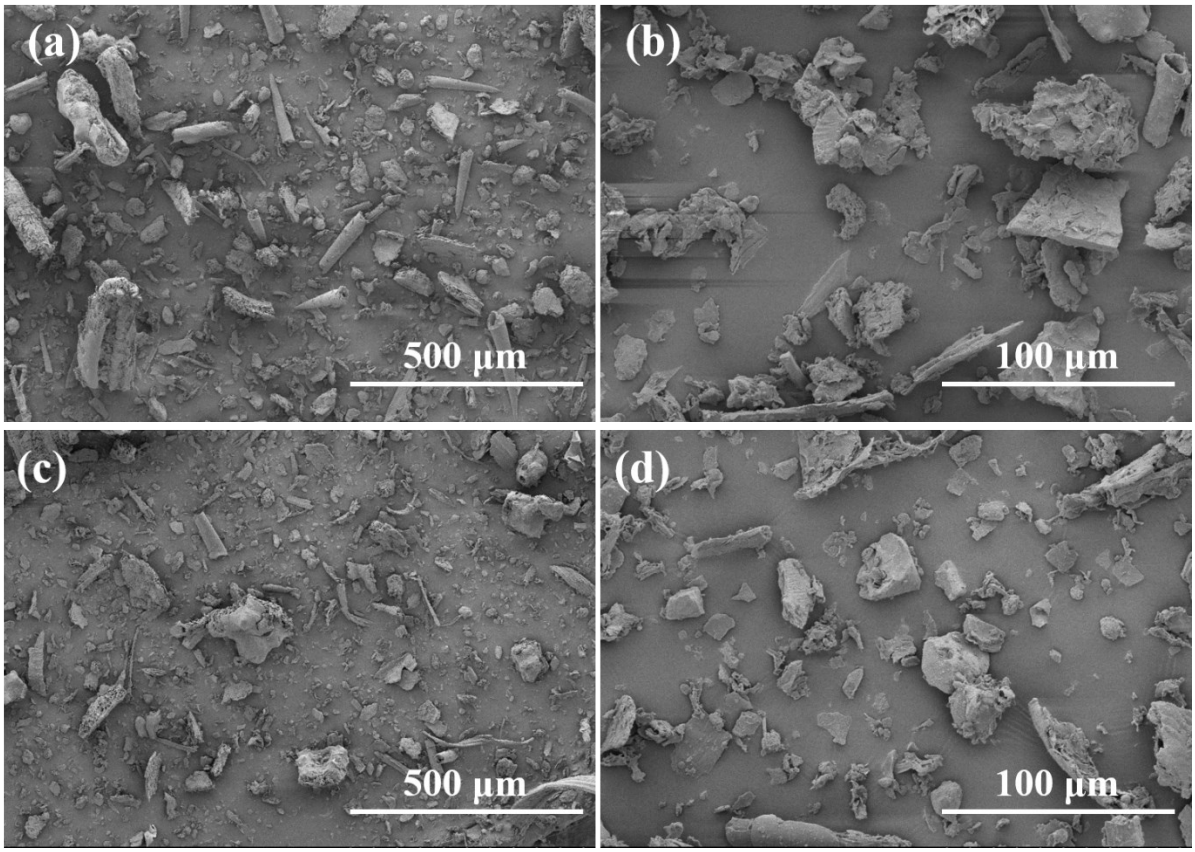

Figure S1. SEM images of (a-b) RH particles, and (c-d) RHB particles at different magnifications.

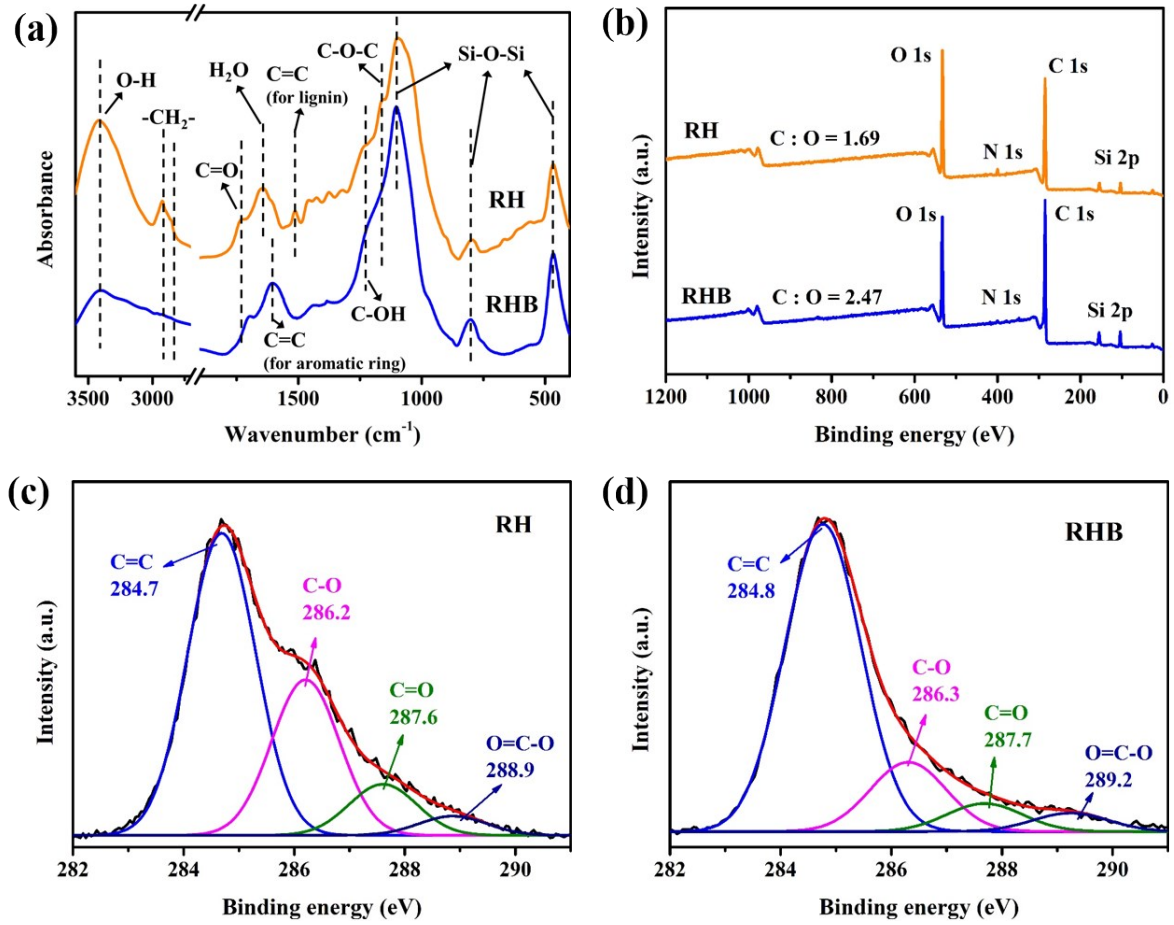

Figure S2. (a) FTIR spectra of RH and RHB particles and (b) XPS survey spectra; detailed deconvolution curves of XPS C 1s for (c) RH, and (d) RHB particles.

To clarify why RHB particles could be an efficient foam stabilizer but RH could not, the microstructure and surface chemical compositions of both particles were characterized and analyzed. Obviously, both RHB and RH particles show similar size ranges and microstructure (Figure S1). The FTIR spectrum of RH shows three characteristic peaks located at 3416, 2900, and 1640 cm^{-1}, which belong to the broad and intense O-H stretching vibration, $-CH_2-$, and water bending mode, respectively. In comparison with that of RH, the peak of aromatic C=C (1600 cm^{-1}) in RHB spectrum becomes stronger, accompanied by the weakening of O-H vibration, $-CH_2-$, and water bending (Figure S2a). The strong peaks at 1100, 796, and 467 cm^{-1} in the FTIR spectra of both RH and RHB particles are attributed to the Si-O-Si bonds, as rice husk is a Si-rich biomass. Moreover, after pyrolysis process at 500 ℃, the ratio of C to O in RHB is increased from 1.69 to 2.47, and the C-O groups on RH decrease significantly, which

also reveal the carbon condensation and crystallization process during pyrolysis, as verified in XPS spectra in Figure S2b-d. The growth of hydrophobic aromatic structure and removal of oxygen-containing groups in RHB suggest that the RHB particles became partially hydrophobic during high temperature pyrolysis. It was reported that one crucial requirement for particles to be a foam stabilizer is that it must be partially hydrophilic/hydrophobic, and then it can adsorb at air-water interfaces to stabilize the bubbles. [1] Therefore, RHB particles with hydrophobic aromatic structure and residual hydrophilic oxygen-containing groups will adsorb at the air-water interfaces as a foam stabilizer. On the other hand, RH particles cannot be adsorbed easily on the interface, because it is hydrophilic and easy absorbing water.

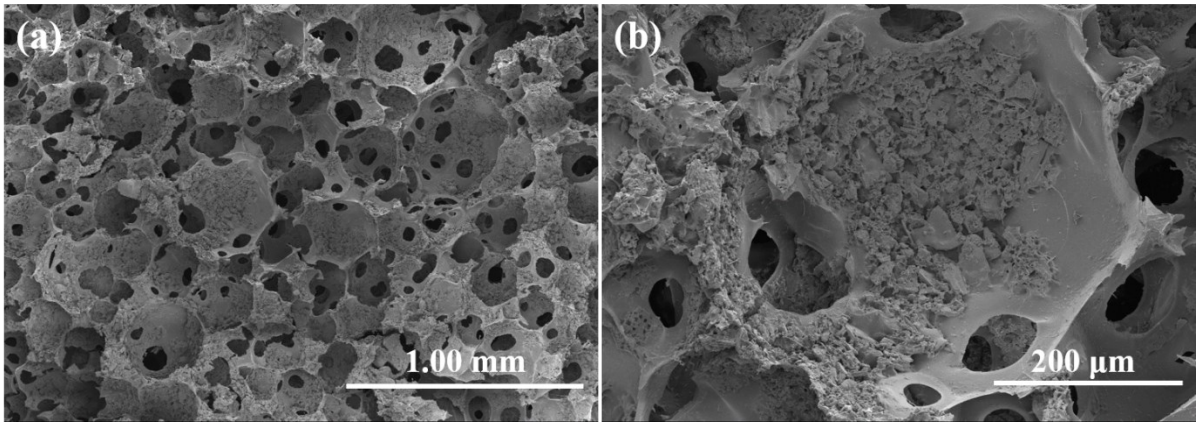

Figure S3. SEM images of RHB-PH.

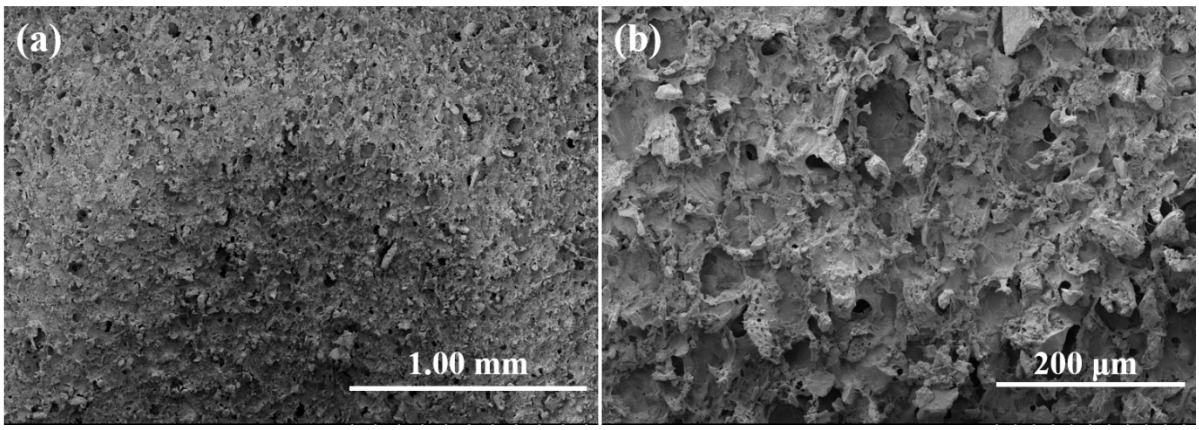

Figure S4. SEM images of RHB-NH.

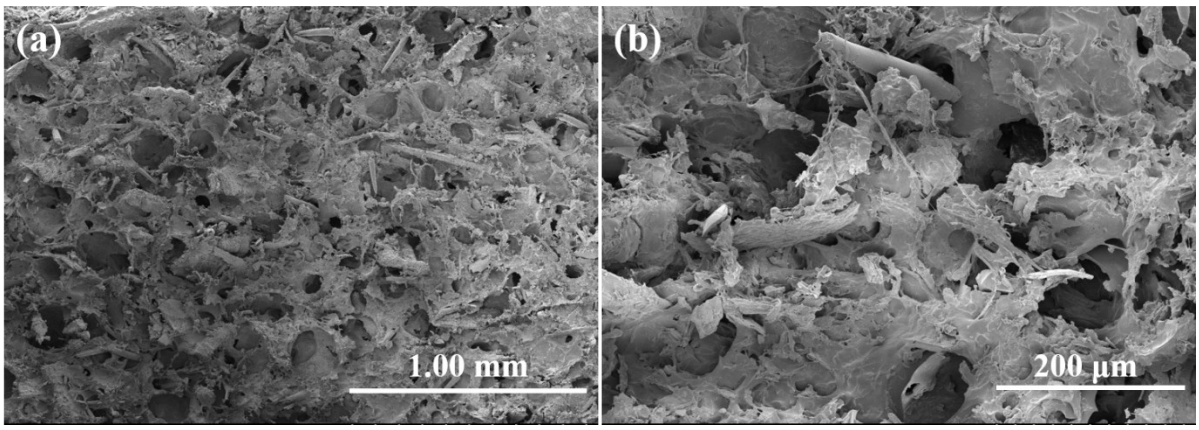

Figure S5. SEM images of RH-H.

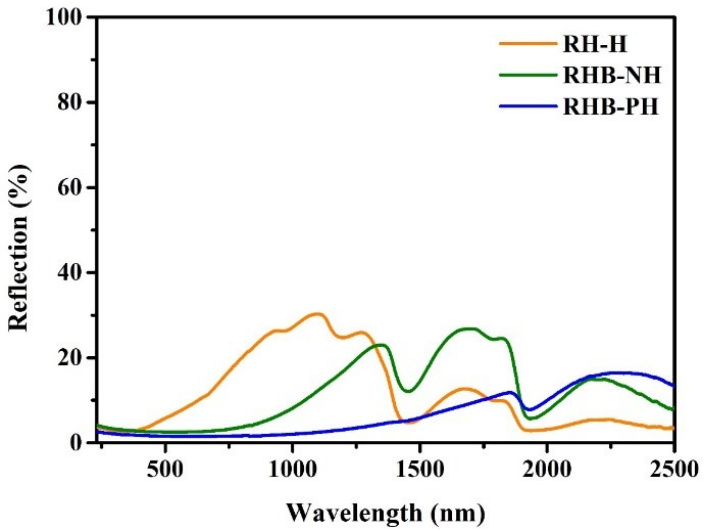

Figure S6. UV-vis-NIR absorption spectra of the carbon-based hydrogels.

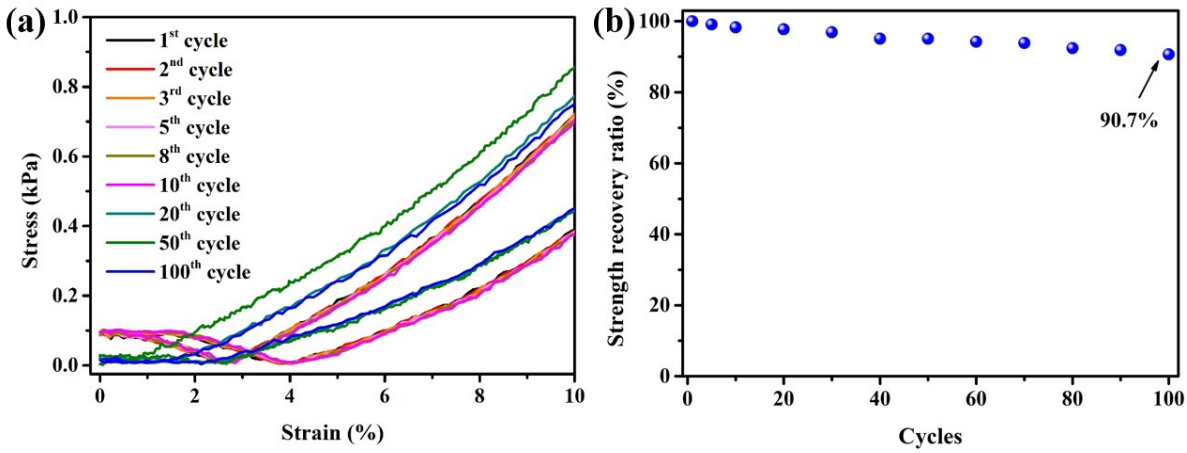

Figure S7. (a) Initial part of the compressive stress-strain curves RHB-PH at 50% maximum strain; (b) corresponding maximum stress recovery during 100 compression cycles (strain at 50%).

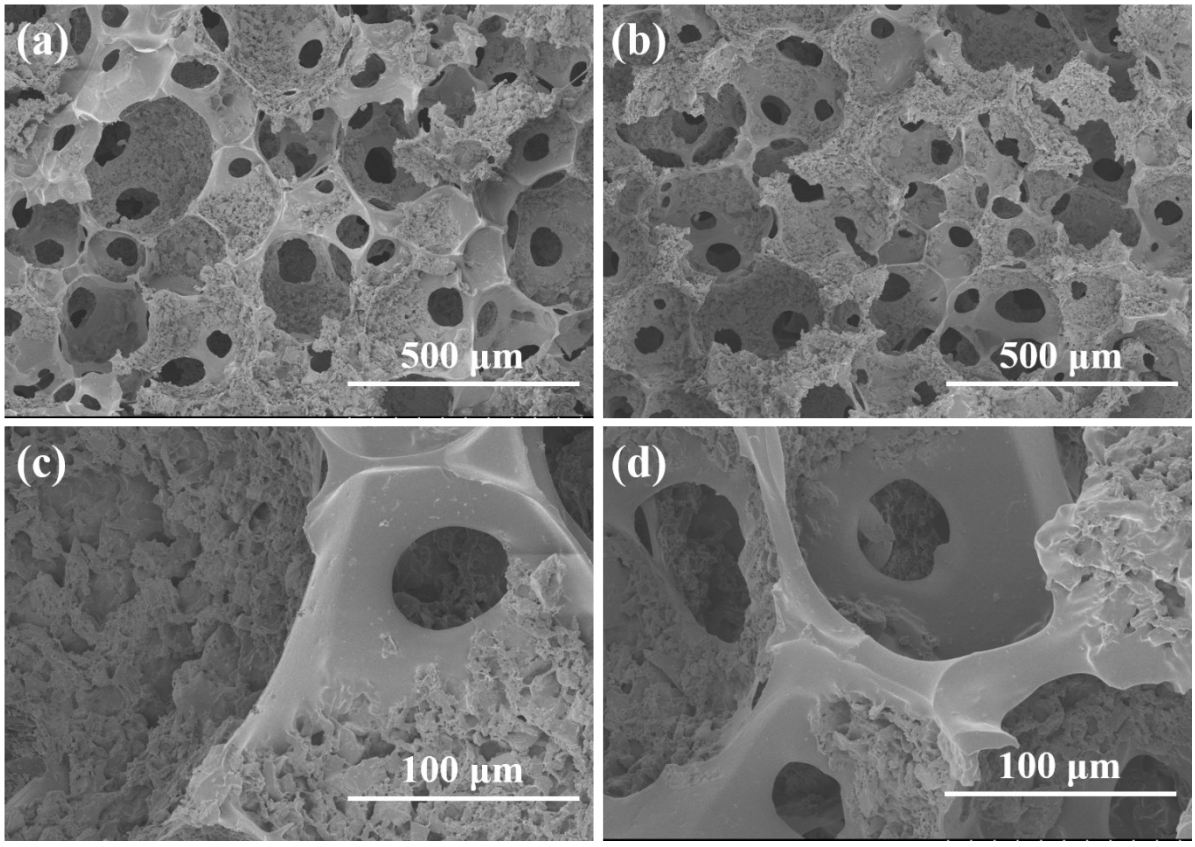

Figure S8. SEM images of RHB-PH after 100 compression cycles at 50% strain.

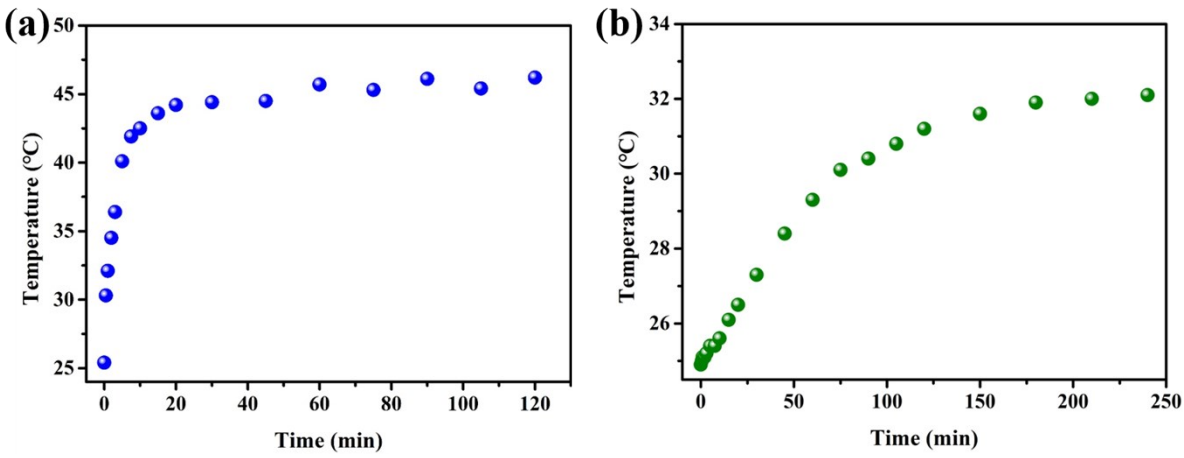

Figure S9. (a) The temperature change curves of RHB-PH surface and (b) corresponding water bulk below the surface under 1-sun illustration.

Generally, the evaporation rate should be no more than 1.47 kg m^{-2} h^{-1}, according to the law of thermodynamics. [2, 3] The excellent evaporation performance of RHB-PH, obviously exceeded the theoretical limit of thermodynamics, should be attributed to the activated intermediate state of water molecules inside the polymeric network. [4, 5] To obtain the real vaporization enthalpy of water inside RHB-PH networks, water and RHB-PH samples with same superficial area were synchronously set in a closed container under room temperature (25 ^{o}C) and ambient air pressure in the dark to guarantee the same energy input.[4, 5] The internal relative humidity (~45%) of container was stabilized by a supersaturated potassium carbonate solution. The equivalent evaporation enthalpy (ΔH_{equ}) of water in RHB-PH can be calculated according to the mass changes of the water samples with identical power input (U_{in}):

$$U_{in} = \Delta H_{vap} \times m_0 = \Delta H_{equ} \times m_g,$$

where ΔH_{vap} and m_0 were the evaporation enthalpy and mass change of bulk water, m_g was the mass change of RHB-PH. The mass changes and calculated ΔH_{equ} were shown in Figure S10. The obtained ΔH_{equ} of water in RHB-PH sample (~ 1981 J g^{-1}) is reduced compared with bulk water (2441.7 J g^{-1}).

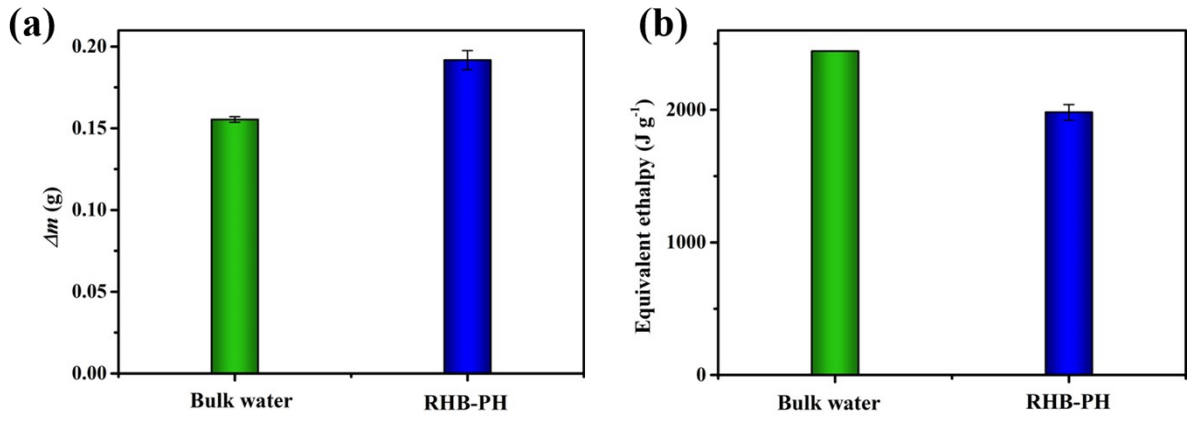

Figure S10. (a) Mass changes of the samples in the container in dark condition after 24 h; (b) the equivalent enthalpy of bulk water and RHB-PH.

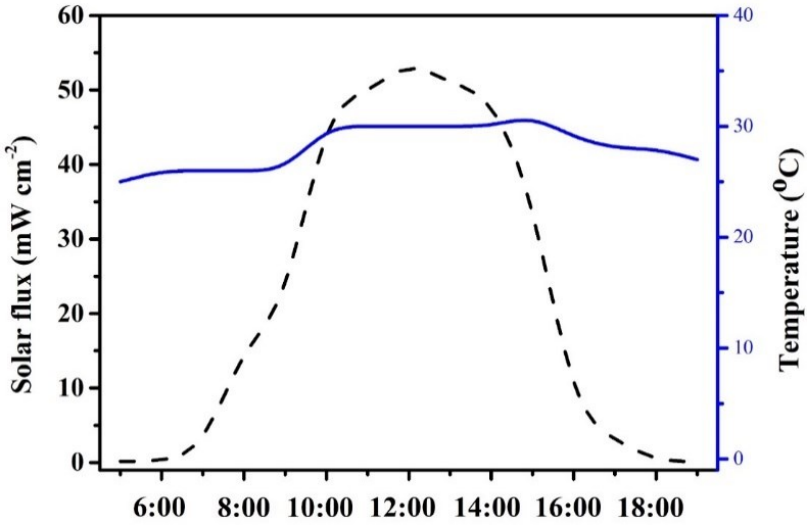

Figure S11. Typical solar flux change during daytime (16th, October) on a sunny day in our institute.

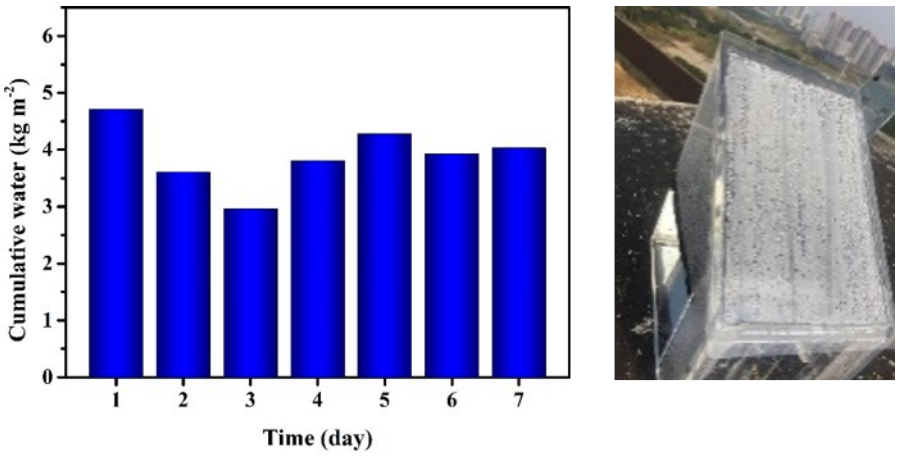

Figure S12. Outdoor performance of RHB-PH as the absorber during 7 days test.

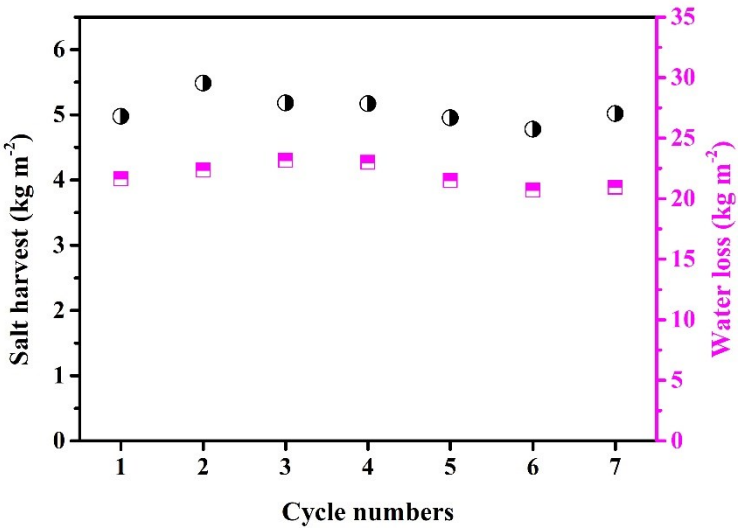

Figure S13. Salt harvest and water loss of RHB-PH evaporator during 7 12-h cycles under 1-sun illustration.

Table S1. Solar evaporation performances based on the biochar-derived sponge-like hydrogel RHB-PH in this work compared with other low cost and widely available carbon-derived materials under 1 kW m^{-2} solar illumination. (deionized water or seawater for short testing time)

Samples	Solar absorption (%)	Evaporation rate (kg m^{-2} h^{-1})	Running time (h)	Ref.
RHB-PH	**93.3**	**1.79±0.008**	**12**	**This work**
Geopolymer-biomass mesoporous carbon composite	90-95	1.58	1	6
Carbonized mushroom	96	1.523	1	7
Glucose-coated carbon fibers	93.0	1.47	1	8
Activated carbon fiber felt	94	1.42	1	9
Carbon-black/cellulose-sponge	97.5	1.40+	0.67	10
Carbon dot/hydrogel	<90	1.40	1	11
Low cost biochar/ethyl cellulose coated filter paper	96	1.37	0.5	12
Wood-derived carbon foam	90.5	1.26	1	13
Biomass-based solar absorber	89.4	1.2	1.5	14
Candle soot coated cotton	\	1.19	1	15
MnO_2/graphene aerogel	~100	1.3542	1	16
MXene aerogel	~96	1.46	12	17

Table S2. Comparison of the solar-driven desalination performances for high concentration brines under 1 kW m^{-2} solar illumination for a long-term experiment.

Samples	Solar absorption (%)	Salt concentration (wt%)	Evaporation rate (kg m^{-2} h^{-1})	Running time (h)	Ref.
RHB-PH	**93.3**	**25**	**1.77±0.05**	**7×12**	**This work**
PVA/graphene hydrogel	~98	25	1.614	4	4
PVA/graphene hydrogel	~98	5-20	2.61-2.21	4	4
MXene aerogel	~96	1.2-7.6	~1.46	15×12	17
Carbon black@Cu foam	~98	10	1.39	8	18
3D solar evaporator	>95	25	1.33	6×20	19
Ti_3C_2 nanosheet	\	2.75	1.31	200	20
Bimodal porous wood (1 sun)	97	15	0.80	\	21
Bimodal porous wood (6 sun)	97	15	6.4	7	21
Glucose-coated Carbon fibers	93.0	10	0.62	3×8	8

References

1. S. Moon, J. Q. Kim, B. Q. Kim, J. Chae and S. Q. Choi, *Chem. Mater.* , 2020, **32**, 4838-4854.
2. W. J. Tu, Z. Z. Wang, Q. Y. Wu, H. Huang, Y. Liu, M. W. Shao, B. W. Yao and Z. H. Kang, *J. Mater. Chem. A*, 2020, **8**, 10260-10268.
3. X. Li, J. Li, J. Lu, N. Xu, C. Chen, X. Min, B. Zhu, H. Li, L. Zhou, S. Zhu, T. Zhang and J. Zhu, *Joule*, 2018, **2**, 1331-1338.
4. X. Zhou, F. Zhao, Y. Guo, Y. Zhang and G. Yu, *Energy Environ. Sci.*, 2018, **11**, 1985-1992.
5. F. Zhao, X. Zhou, Y. Shi, X. Qian, M. Alexander, X. Zhao, S. Mendez, R. Yang, L. Qu and G. Yu, *Nat. Nanotechnol.*, 2018, **13**, 489-495.
6. F. Liu, B. Zhao, W. Wu, H. Yang, Y. Ning, Y. Lai and R. Bradley, *Adv. Funct. Mater.*, 2018, **28**, 1803266 (1803261-1803211).
7. N. Xu, X. Hu, W. Xu, X. Li, L. Zhou, S. Zhu and J. Zhu, *Adv. Mater.*, 2017, **29**, 1606762 (1606761-1606765).
8. T. Li, Q. Fang, X. Xi, Y. Chen and F. Liu, *J. Mater. Chem. A*, 2019, **7**, 586-593.
9. H. Li, Y. He, Y. Hu and X. Wang, *ACS Appl. Mater. Interfaces*, 2018, **10**, 9362-9368.
10. S. Liu, C. L. Huang, Q. Q. Huang, F. C. Wang and C. W. Guo, *J. Mater. Chem. A*, 2019, **7**, 17954-17965.
11. S. Singh, N. Shauloff and R. Jelinek, *ACS Sustainable Chem. Eng.*, 2019, **7**, 13186-13194.
12. J. L. Li, M. H. Du, G. X. Lv, L. Zhou, X. Q. Li, L. Bertoluzzi, C. H. Liu, S. N. Zhu and J. Zhu, *Adv. Mater.*, 2018, **30**, 1805159 (1805151-1805157).
13. P. X. Qiu, F. L. Liu, C. M. Xu, H. Chen, F. Jiang, Y. Li and Z. B. Guo, *J. Mater. Chem. A*, 2019, **7**, 13036-13042.
14. Q. Fang, T. Li, Z. Chen, H. Lin, P. Wang and F. Liu, *ACS Appl. Mater Interfaces*, 2019, **11**, 10672-10679.
15. H. M. Wilson, A. R. S. Rahman, A. E. Parab and N. Jha, *Desalination*, 2019, **456**, 85-96.
16. Z. Zhang, P. Mu, J. X. Han, J. X. He, Z. Q. Zhu, H. X. Sun, W. D. Liang and A. Li, *J. Mater. Chem. A*, 2019, **7**, 18092-18099.
17. Q. Zhang, G. Yi, Z. Fu, H. T. Yu, S. Chen and X. Quan, *ACS Nano*, 2019, **13**, 13196-13207.

18. N. Xu, J. L. Li, Y. Wang, C. Fang, X. Q. Li, Y. X. Wang, L. Zhou, B. Zhu, Z. Wu, S. N. Zhu and J. Zhu, *Sci. Adv.*, 2019, **5**, 7013 (7011-7017).

19. Y. Shi, C. Zhang, R. Li, S. Zhuo, Y. Jin, L. Shi, S. Hong, J. Chang, C. Ong and P. Wang, *Environ. Sci. Technol.*, 2018, **52**, 11822-11830.

20. J. Q. Zhao, Y. W. Yang, C. H. Yang, Y. P. Tian, Y. Han, J. Liu, X. T. Yin and W. X. Que, *J. Mater. Chem. A*, 2018, **6**, 16196-16204.

21. S. M. He, C. J. Chen, Y. D. Kuang, R. Y. Mi, Y. Liu, Y. Pei, W. Q. Kong, W. T. Gan, H. Xie, E. Hitz, C. Jia, X. Chen, A. Gong, J. M. Liao, J. Li, Z. J. Ren, B. Yang, S. Das and L. B. Hu, *Energy Environ. Sci.*, 2019, **12**, 1558-1567.